Journal of the European Ceramic Society **15** (1995) 605–615

0955-2219/95/$9.50
0955-2219(95)00025-9

The Barrier Height Formation in ZnO Varistors

P. Q. Mantas & J. L. Baptista

Dep^{to} Eng.^{a} Cerâmica e do Vidro (INESC), Universidade de Aveiro, 3800 Aveiro, Portugal

(Received 2 June 1994; revised version received 27 January 1995; accepted 31 January 1995)

Abstract

The electrical characteristics of ZnO ceramic varistors are interpreted as being due to the existence of potential barriers at the grain boundaries. The two main models describing the origin of these barriers, surface states at the interface, and surface oxidation, are discussed in this work, where the microstructure and the electrical properties at various temperatures (up to 160°C) of a standard varistor composition, are used in an attempt to separate both contributions. The temperature dependence of both the distribution of surface states and the Fermi level, when extrapolated to high temperatures, indicates that the surface states control mainly the shape of the I–V curves, and that the surface oxidation contribution to the barrier, although as high as 0·25 eV, is not sufficient to account for the total energy of the barrier. Values for the density of carriers calculated using the dependence of the Fermi level on temperature, were in good agreement with reported values determined by other techniques.

1 Introduction

The electrical characteristics of ZnO varistors are interpreted as due to potential barriers formed at the grain boundaries of the ceramic material. There are two main models describing the origin of these barriers: (i) surface states at the interface, and (ii) surface oxidation. In the first model, it is considered that the junction between two semiconducting ZnO grains (n-type semiconductor at room temperature) behaves as a p-type semiconductor, and, for the thermodynamic equilibrium, i.e. the equalisation of the Fermi level throughout the junction, a process of charge transfer between the grains and the interface is necessary.[1,2] As a consequence of this process, donors in the grains nearby the interface are ionized, giving electrons to the interface states, which also become ionized. The region near the junction is depleted of charges, and therefore, a potential barrier appears. In equilibrium, there is a simple relation between these three entities, the barrier height, Φ_{Bo}, the ionized donors, N_D, and the ionized charge at the interface, Q_{io}: $\Phi_{Bo} \propto Q_{io}^2/N_D$. Since two opposite Schottky type barriers are formed, this model is also called the Double Schottky Barrier (DSB) model.

In the second model, it is considered that the regions of the ZnO grains near the grain boundaries are much more resistive than the bulk of the grains. The difference in resistivities is due to a non-equilibrium defect chemistry process, arising during the cooling down period. At the sintering temperature (>1200°C), all the material can be considered in thermodynamic equilibrium, and so there is a great concentration of defects, namely those of the Schottky type. When the sample is cooled, these defects must diffuse from the bulk of the grains to the surface where they will be annihilated. Because both the defect formation and the defect diffusion are thermally activated, only the defects near the grains surface are able to reach the interface to be annihilated, the others being frozen in the bulk. The bulk of the grains remains with a high concentration of defects (giving the n-type semiconductor nature), while the interface becomes stoichiometric, i.e. highly resistive (the forbidden band in ZnO at room temperature is about 3·2 eV). For the electron flow across such a junction, a potential barrier is therefore present.[3,4]

Both models, n–p–n and n–i–n, reasonably describe the I–V curves of these materials, if the varistor quality factor α is less than ~25.[5] For higher α values, they need to incorporate other mechanisms of electron flow, based on impact ionization[6–9] or electron tunneling from one grain to the other.[10,11]

In this work we used ZnO varistor samples to measure their electrical characteristics at several temperatures, up to 160°C, and used these experimental results to theoretically derive the distribution of surface states above the equilibrium Fermi level, in an attempt to differentiate the contributions from the two mechanisms for the formation of the varistor potential barriers.

2 Experimental

Varistor samples prepared via a normal ceramic processing route, and sintered at 1300°C, 1 h, in air, were used. The chemical composition of these samples was: 97·0 mol% ZnO and 3·0 mol% of Bi_2O_3, Sb_2O_3, Co_2O_3, MnO_2 and Cr_2O_3, with the molar proportion of 1:2:1:1:1. Samples were used for SEM observation, after polishing and chemically etching the surfaces. Mean grain size was determined by the interseption method, using a computer aided system. Samples used for electrical measurements were sputtered on opposite faces with gold electrodes, after lapping. Electrical measurements were preformed in an oven, heated via an electrically heated wire double wound around a supporting tube. A wire net was used to shield the sample from the tube. Temperatures were controlled with the aid of a programable controller, using cromel–alumel thermocouples. Before electrical measurements, the temperature in the oven was stabilized for 30 min.

I–V measurements were made with a current source (Keithly 225 Current Source), and an electrometer (Keithly 616 Digital Electrometer), up to 100 V. At room temperature, for higher voltages, a pulsed source (AMBO, with 60 μs pulse duration, 13 Hz, up to 1 kV) was used. C–V measurements were done with an ac bridge (Hewlett-Packard 4280A 1MHz C Meter/C-V Plotter), at a fixed frequency of 1 MHz, up to 40 V dc applied voltage.

3 Results and Discussion

3.1 Microstructure

Figures 1 and 2 show the microstructure of the varistor; it can be seen that three phases are present: large ZnO grains, inter/intragranular spinel particles, and a third minor phase, brighter than the other two, that is possibly the reported pyrochlore type phase.[12–18] By EDS, we could hardly detect the presence of Co as the only dopant inside the ZnO grains (Fig. 3(a)). The spinel phase is doped with Co, Mn, and Cr (Fig. 3(b)). The third phase is composed by Zn, Sb, and Bi (Figs 3(c) and 2). This type of microstructure is the one that could be expected from the chemical composition of the sample and the sintering schedule used, as reported by Inada.[13–15] However, it must be

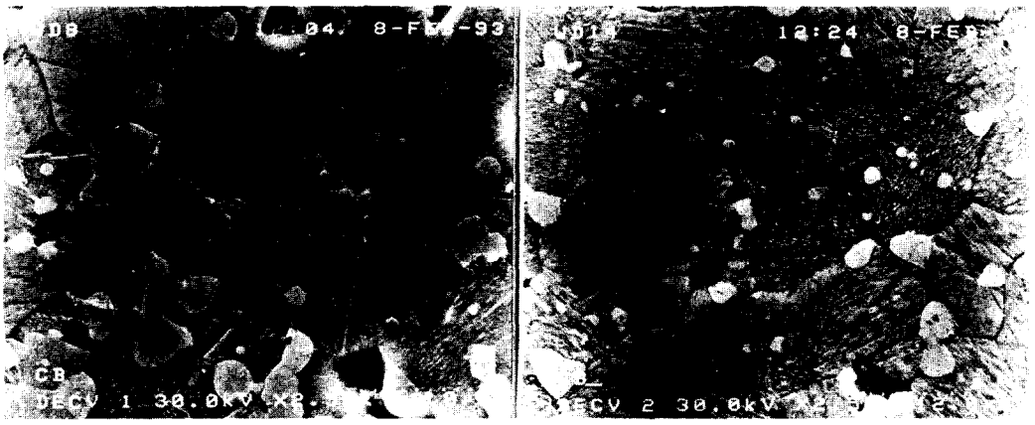

Fig. 1. SEM micrograph of polished and chemically etched sample. The spinel like phase (A) is normally located at the grain boundaries of the ZnO grains with some finer particles inside the grains. A brighter phase (B) can be found near the spinel like phase, and is probably the reported pyrochlore type phase.

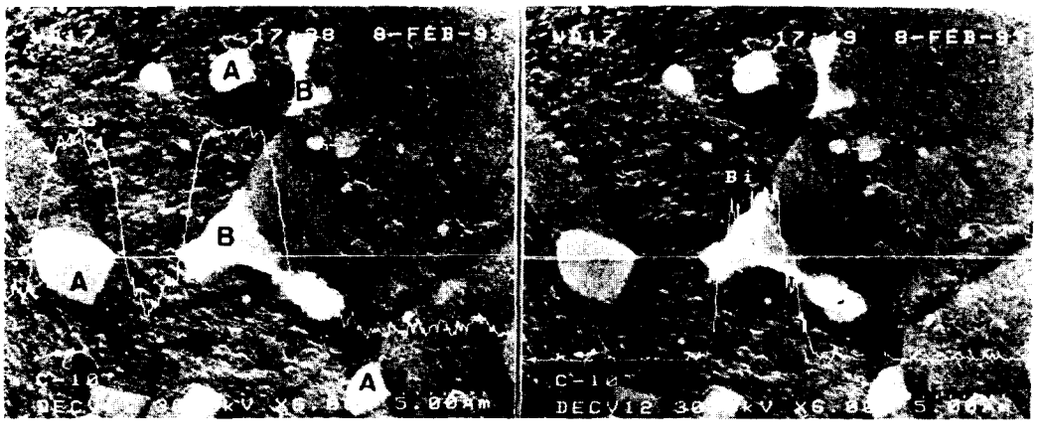

Fig. 2. Antimony and bismuth profiles (by EDS attached to the SEM) of the three phases present in the sample microstructure. Both the spinel like phase (A) and the brighter phase (B) contain Sb, while Bi is only present in the brighter phase.

emphasized that Co, Mn or Cr, were not detected in the third phase. If this phase is the pyrochlore type phase, then it comes with ZnO from the reaction between the spinel like and the Bi-rich liquid phases, during the cooling down of the sample[13–15]

$$3Zn_7Sb_2O_{12}(SP) + 3Bi_2O_3(Liq.) \xrightarrow{950°C} 4Bi_{3/2}ZnSb_{3/2}O_7(PY) + 17ZnO \quad (1)$$

where SP is spinel and PY pyrochlore.

Since the third phase does not contain Co, Mn or Cr, it is possible that these dopants were incorporated in the newly precipitated ZnO. Einzinger[3,4] and Schwing and Hoffmann,[10,11] proposed the build up of the potential barrier in the ZnO grain boundaries as being due to the presence of Co in the grain boundary. For these authors, this mechanism is important for the build up of the potential barrier in the grain boundaries, since foreign atoms segregated near the interface will shift the relative concentrations of zinc and oxygen vacancies. Donor cations (Co, Mn or Cr) will decrease the oxygen vacancy concentration relative to that of zinc vacancy and, consequently, the Fermi level at the interface will be lower in energy, relative to the conduction band edge, than in the bulk of the material; this means that a potential barrier is formed at the interface. The above results could support this mechanism, since a high concentration of these dopants would be in the

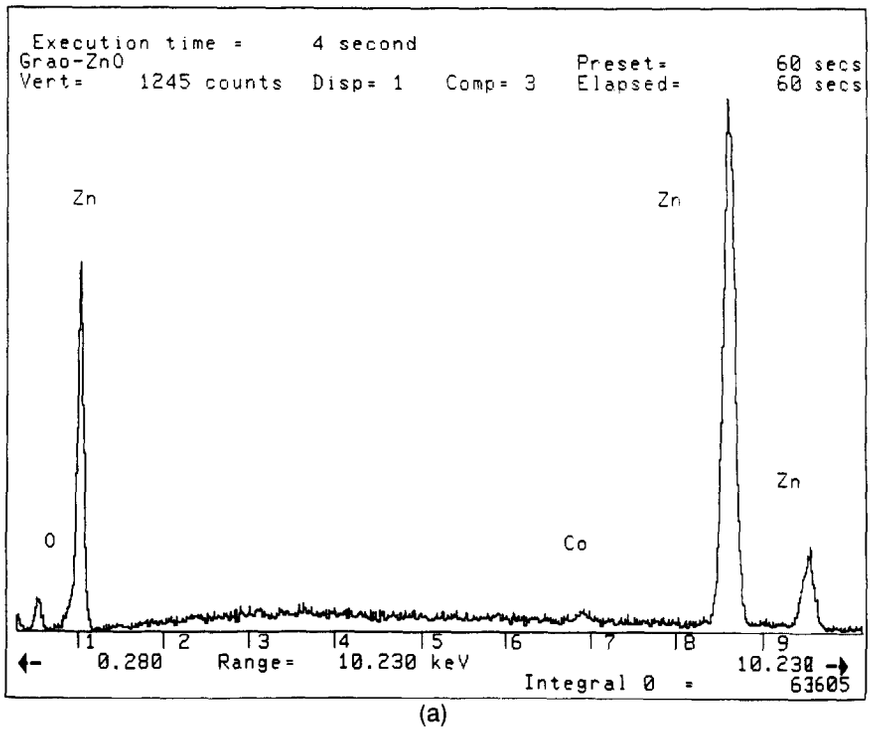

(a)

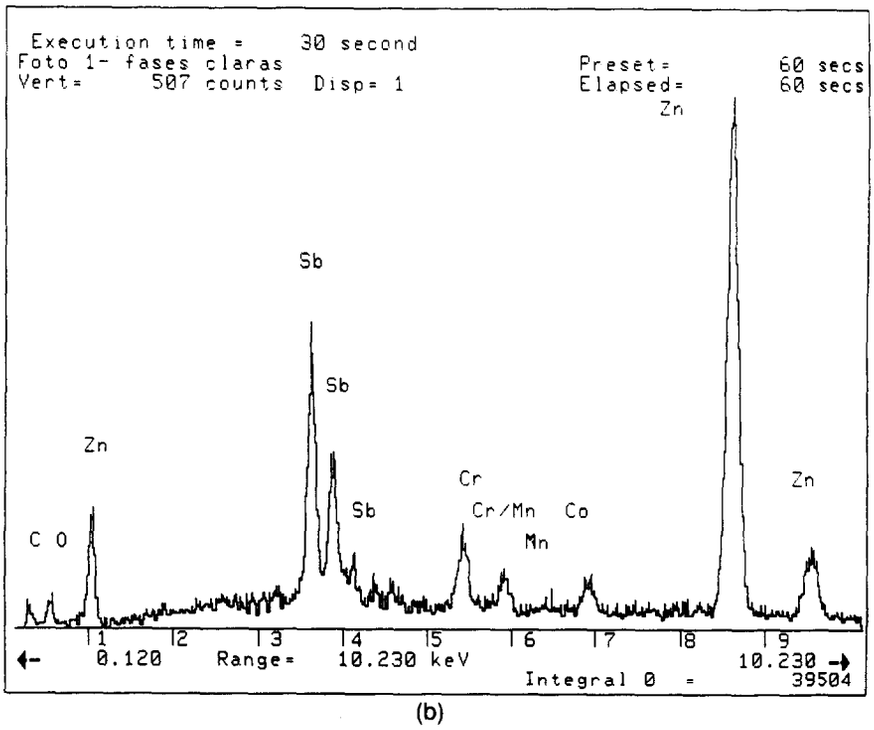

(b)

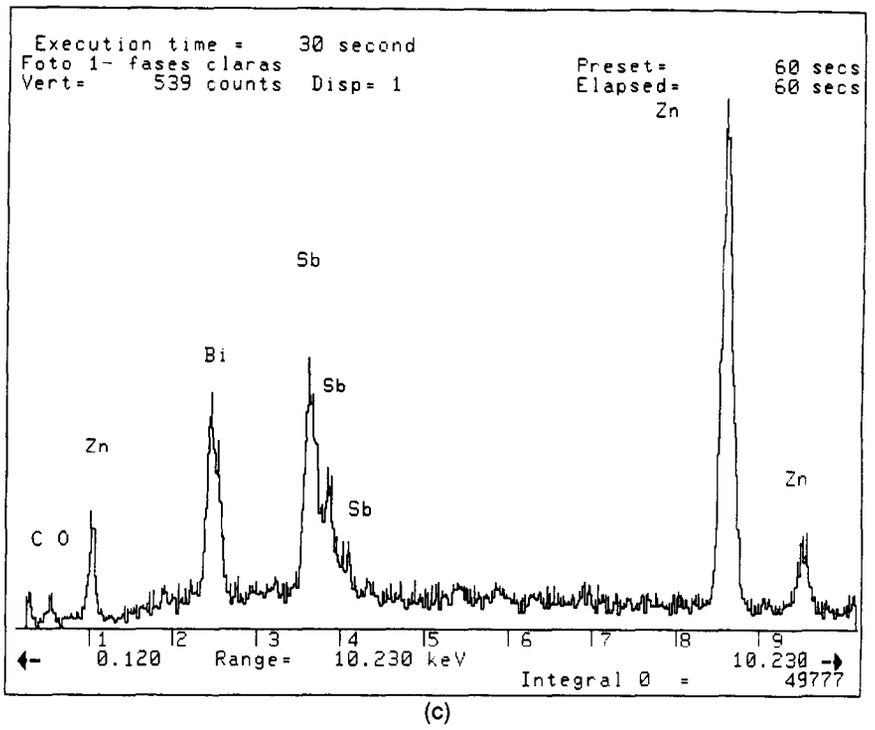

Fig. 3. EDS spectra of the three phases present in the sample microstructure: (A) ZnO phase, showing faintly the presence of Co; (B) spinel like phase, doped with Cr, Co, and Mn; and (C) the brighter phase, composed by Zn, Sb, and Bi, without clear evidence of the dopants.

freshly precipitated ZnO layer. However, in this temperature range (~950°C), most of the ZnO–ZnO grain boundaries are already formed and the material already presents varistor characteristics,[19] and so some doubts can be put on accepting this mechanism as the main contribution to the formation of the potential barriers. It was decided, therefore, to pursue this matter in some detail, and see if there was consistency between the DSB model and the formation mechanism of the potential barriers.

3.2 Varistor parameters

3.2.1 The method used to determine the density of surface states (DOS)

In this work, we firstly determined the equilibrium Fermi level at the interface, E_{Fo}, and thereafter the density of surface states (DOS), at various temperatures, ranging from room temperature up to 160°C. Both parameters, E_{Fo} and DOS, were calculated from each experimentally determined I–V curve, using the double Schottky barrier model (DSB). The procedure was made by successive fittings of the theoretically calculated I–V curves to the experimental ones, until a good fitting between both curves was found. In the following, we describe this procedure step by step.

Using the DSB model, there are two main steps to obtain the electrical parameters that allow the derivation of the I–V curves: in the first step, the relation between the barrier height, Φ_B, and the applied voltage across one junction, V, is found; in the second one, these two parameters are related with the electron flux, J_{DC}. Once the I–V curve is obtained for one junction, it is necessary to relate it to the polyjunction system describing the polycrystalline material. We shall return to this last relation later in this section.

To accomplish the first step, it is necessary to know the density of charge in the junction, $\rho(x)$, and solve the Poisson equation for that case. This has been done by Blatter and Greuter[20,21] who have found a relatively simple relation between the barrier height and the applied voltage

$$\Phi_B = \frac{V_C}{4}\left(1 - \frac{V}{V_C}\right)^2 + \sum_{\nu=1}^{n} N_\nu(\epsilon_\nu - \epsilon_\xi)\left(e\sum_{\nu=0}^{n} N_\nu\right)^{-1} \quad (2)$$

In this equation, the critical voltage, V_C, is related to the accumulated charge at the interface, Q_i, and to the concentration of donors in the grains, N_ν, by the equation

$$V_C = Q_i^2\,(2\epsilon\epsilon_o e\sum_{\nu=0}^{n} N_\nu)^{-1} \quad (3)$$

where ϵ is the relative permitivity of the material, ϵ_o the vacuum permitivity, and e the electron charge. Each donor species, ν, with density N_ν, is in the energy level $E_g - \epsilon_\nu$, where E_g is the forbidden band of the semiconductor; $E_g - \epsilon_\xi$ is the Fermi level in the bulk of the material. The second term of the right hand side in eqn (2), is the contribution of deep donor levels to the barrier height. These

deep levels tend to decrease the barrier height, and have some effect in the I–V curves for high voltages (normally in the breakdown region). As has been pointed out,[20,21] for normal densities of deep levels in ZnO varistors (ca. 10% of the density of shallow donors), the barrier height is reduced by ~0·10 eV, which only represents 10%–20% of the total barrier height; moreover, experimentally it is difficult to observe any smooth change of the I–V curve at high voltages, especially in the breakdown region. Because of that, we have neglected this type of contribution, and so eqn (2) reduces to quite a simple one

$$\Phi_B = \frac{V_C}{4}\left(1 - \frac{V}{V_C}\right)^2 \tag{4}$$

The accumulated charge at the interface, Q_i, represents the total amount of trapped charge,

$$Q_i = e\int_{\xi_i^n}^{n} N_i(E) f_i(E)\,dE \tag{5}$$

where ξ_i^n is a fictitious Fermi level describing the neutral interface, $N_i(E)$ the density of surface states, and $f_i(E)$ their probability of being occupied. Upon the application of the voltage, some of the surface states are ionized, and so the Fermi level at the interface shifts upwards in energy. The voltage dependent barrier height is defined by eqn (2) (or (4)) and by $e\Phi_B(V) = E_g - \epsilon_\xi - E_F(V)$; so any pair of ($\Phi_B$, V) values must be found in a self-consistent way.[20,21]

In the second step for the determination of the I–V curve, it was assumed that the electron flux over the barrier corresponds to the thermionic emission mechanism.[1,2,20,21] It has been shown by Pike[22] that a diffusion mechanism will give similar results, so both mechanisms can be applied to describe the system. Other mechanisms, like the field emission, used by other authors,[23] were not considered here. According to the thermionic emission mechanism, the electrical density across a junction has the form

$$J_{DC} = A^*T^2\exp(-(e\Phi_B(V)+\epsilon_\xi)/kT)(1-\exp(-eV/kT)) \tag{6}$$

where A* is the Richardson constant, T the absolute temperature, e the electron charge, and k the Boltzmann constant; [1– exp(–eV/kT)] corresponds to the net electron flux crossing the junction.[1,2,20,21] In a more accurate description, the electron capture probability must also be taken into consideration in this equation, but since this is a rather minor correction, we have neglected it.[20,21]

Having defined the relation between applied voltage and current density for one junction, i.e. the I–V curve, it is important to relate this to the material characteristics. It is normally accepted that the I–V properties of the material can be described by an equivalent electrical circuit composed of a network or resistors. It is also known that some of the grain boundaries in the material are not electrically active, i.e. they don't have varistor properties. It has been proposed[24] that in such equivalent circuits, it is only necessary to have ~30% of good electrical junctions for the material to behave as a varistor. In view of this result, one can consider that the material is composed of a series of resistors between the electrodes, whose number, m, can be readily calculated by $m \approx d/G$ (d being the sample thickness, and G the mean grain size of the material). This type of approximation can give values of 2–3 volts per grain boundary (V/GB) for the breakdown voltage. If, experimentally, a varistor has α values greater than 25, it is necessary to incorporate a mechanism of impact ionization, or a tunneling mechanism, as already pointed above. For these mechanisms to operate, the breakdown voltage must be ≥3·2 V/GB. This value has been found experimentally for one junction, using microcontacts over a polished surface;[25–28] besides, it is the threshold voltage for the mechanism of impact ionization, also found experimentally.[7] This means that the approximation used for the determination of m, where every grain boundary was counted, can give unrealistic results. However, in these situations where $\alpha \geq 25$, the number of electrically active grain boundaries, m', can be easily found by assuming that the 3·2 V/GB have been reached for these samples, which allows the use of the relation $V_{breakdown}/m' \approx 3{\cdot}2$ V/GB. Once this value has been found, it is thus possible to compare the theoretically calculated (J_{DC}, V) curve with the experimental (J_{DC}, V_{exp}/m') one.

Knowing the relevant electrical parameters for each case, it is then possible to fit a theoretically calculated I–V curve to the experimental one, by manipulating only the distribution of the surface states. In this work, we made this approach with the aid of a computer program, in which the density of surface states (DOS) was introduced as a set of Gaussian distributions. In practice, the type of distribution used is not important, since we could input any number of Gaussians and integrate them to fit the curves.

Since we neglected the contribution of deep donors to the barrier height, N_ν reduces to N_0 (ν = 0). For the density of ionized donors. N_0, we used the values determined by the known relation:[29]

$$\left(\frac{1}{C} - \frac{1}{2C_0}\right)^2 = \frac{2(\Phi_B + V)}{e^2\epsilon\epsilon_0 N_D} \tag{7}$$

where C and C_0 are the capacitance at V and $V = 0$

applied voltage, respectively, and N_D the total density of ionized donors. We assumed that $N_0 \equiv N_D$, since this relation was used with results obtained at a fixed frequency of 1 MHz.[1,3,20,21]

3.2.2 Electrical characteristics

To plot the I–V curves, V/GB was determined by $V_{applied}/m$, where $V_{applied}$ is the voltage applied to the sample, and m is the total number of grain boundaries between the electrodes, m = 189 (with G = 9·8 μm). For this value of m, at a current density of 0·5 mA/mm^2, which is the current density normally accepted for the onset of the breakdown regime,[30] V/GB $\approx$ 2·6 V, and the α value is greater than 25, $\alpha \approx 35$. As already said, for such a high value of α, the voltage applied to each grain boundary exceeds 3·2 V. The calculated value, 2·6 V, is lower than this one, and we can presume that not all the grain boundaries are electrically active. Assuming that this value must be at least 3·2 V, then the number of electrically active grain boundaries is m' = 152. Figure 4 shows the I–V curves, plotted as ln(J) versus ln($V_{applied}/m'$), where J is the current density, for the various temperatures. In this figure m' = 152, which corresponds to ~80% of good junctions in the material and is far above the minimum required for the varistor action. This fraction of good junctions in the material seems to be too high to correspond to the mechanism of segregation of dopants in the ZnO–ZnO boundaries via the formation of the pyrochlore phase by eqn (1), since this phase is a rather minor one, and most of the ZnO grain boundaries must be already formed at ~950°C.[19]

The next step is the determination of the energy of the equilibrium Fermi level at the interface, E_{Fo}, at each temperature. At zero bias, i.e. for lim J_{DC} (V→0) in eqn (6)

$$\sigma = ek^{-1}A^*T\exp[-(e\Phi_{Bo} + \epsilon_\xi)/kT] \qquad (8)$$

and the conductivity, σ, of the material depends essentially on the exponential part of eqn (8). Since $E_{Fo} = E_g - (e\Phi_{Bo} + \epsilon_\xi)$, then E_{Fo} determines the conductivity of the material at each temperature. Assuming a reasonable value for the bulk Fermi energy, ϵ_ξ, E_{Fo} can be calculated for each temperature by simply fitting the ohmic highly resistive part of the I–V curve to the theoretically calculated one. We assumed that ϵ_ξ = 0·05 eV for all the tested temperatures; it is a reasonable energy for the semiconductor, although not necessarily constant for all temperatures. The choice of this energy is to be checked in the following.

Figure 5 represents the variation of E_{Fo} with temperature. It is an almost straight line, with slop $dE_{Fo}/dT = -2{\cdot}3 \times 10^{-3}$ eV K^{-1}. Rossinelli *et al.*[31] have found a similar value for the $SrTiO_3$ based varistors ($-2{\cdot}0 \times 10^{-3}$ eV K^{-1}), and in view of the two quite different chemical systems, it is expected that they have the same physical origin. During heating, the width of the ZnO forbidden band is also decreasing, $E_g = E_{go} - \beta T$, with β = 9·5 × 10^{-4} eV K^{-1}.[32] Instead of calculating the absolute change of E_{Fo} with temperature, we have calculated the relative change of E_{Fo} to E_g with temperature. For each temperature we plotted E_{Fo}/E_g–vs–T, and have then calculated the slope of the obtained curve. We found $d(E_{Fo}/E_g)/dT = -5{\cdot}2 \times 10^{-4}$ K^{-1}. Such temperature dependence can be

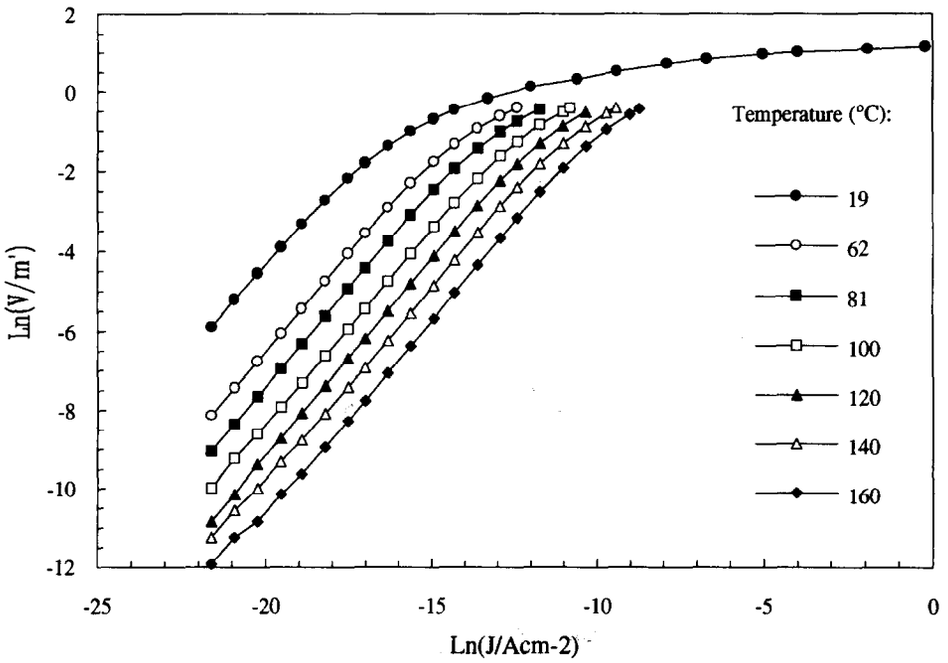

Fig. 4. I–V curves of the samples at the studied temperatures (legend inside the figure). In this Figure, V/GB was determined by $V_{applied}/m'$, where m' = 152 is the number of good junctions (see text).

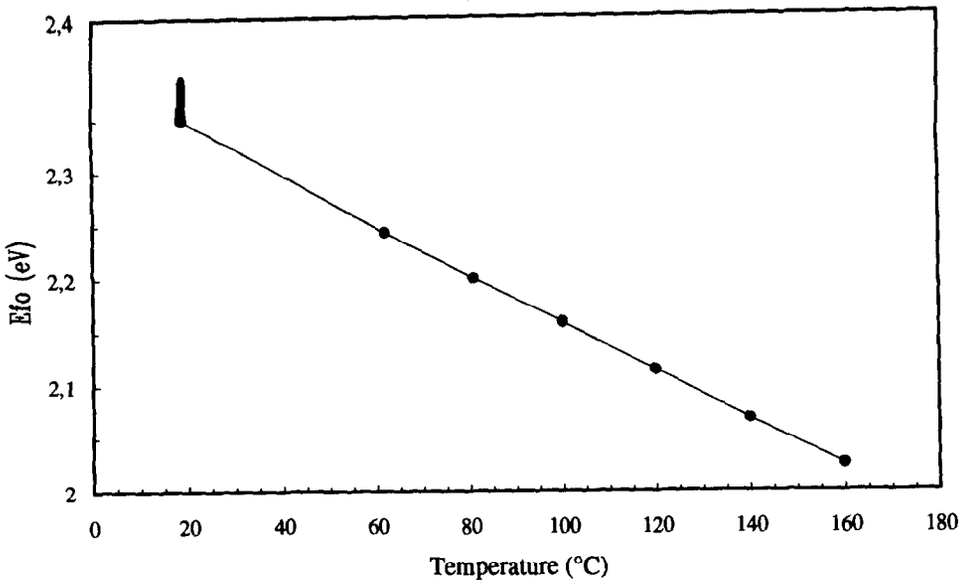

Fig. 5. Variation of the equilibrium Fermi level at the interface, E_{Fo}, with temperature.

assigned to the variation of the bulk Fermi level, assuming that the density of carriers in the ZnO conduction band, in this temperature range, is controlled by donor defects (either intrinsic, like the zinc interstitial, Zn_i, or the oxygen vacancy, V_O, or extrinsic, e.g. due to the presence of Co). As a first approximation, the density of carriers, n, can be considered constant,[33] and ϵ_ξ can be determined by adjusting the n value in the following eqn (9), until it has the same temperature dependence as E_{Fo}/E_g

$$\epsilon_\xi = kT\ln\left(\frac{N_C}{n}\right) \tag{9}$$

where $N_C = 2(2\pi m_e^* kT/h^2)^{3/2}.m_e^*$ is the electron effective mass in ZnO, taken as $m_e^* = 0{\cdot}25m_o$, and h is Planck's constant. Equation (9) is, of course, not entirely correct, since the exact structure of the system is not known (type of donor species, its energy and concentration). However, it gives quite reasonable values for n and for ϵ_ξ: (i) the adjusted n value, $n = 4{\cdot}5 \times 10^{16}$ cm^{-3}, is in close agreement with values determined by other techniques (infrared spectroscopy,[34] high current and high frequency measurements[35]) on commercial varistor samples, $n \sim 1 \times 10^{17}$ cm^{-3}, and (ii) the value of the bulk Fermi level, ϵ_ξ, ranges from 0·10 eV, at room temperature, up to 0·18 eV, at 160°C, values which fall in the range of 0·066 eV[20,21] to 0·32 eV.[36] Knowing the values of E_{Fo} and ϵ_ξ for each temperature, we are now able to calculate the density of states (DOS).

To calculate the DOS we used the parameters listed in Table 1. Figure 6 shows the DOS as a function of the energy at the interface, for all the tested temperatures. For these calculations we introduced four Gaussian curves for each temperature. One of these curves, E_1 in Table 2, corresponds mostly to the ionized surface states in equilibrium, i.e. to Q_{io}. Although the density and distribution of the DOS below the equilibrium Fermi level cannot be known be this method, it is however necessary to use Gaussian curves that extend below the equilibrium Fermi level in order that the DOS very close to it (above and below) can be computed to correctly calculate the DOS for higher energies. This is the reason why this Gaussian curve is shown in Table 2. The Table also shows the parameters of the Gaussian curves, E_i, σ_i, and N_i, representing the energy level, the standard deviation, and the total surface states, respectively, for each tested temperature. It must

Table 1. Used and calculated electrical parameters for the determination of the DOS: the energy of the band gap, E_g, bulk Fermi level, ϵ_ξ, and the concentration of donor species, N_D, were used to calculate the equilibrium values for the interface Fermi level, E_{Fo}, barrier height, Φ_{Bo}, and trapped charge at the interface, Q_{io}. Other important parameters are: electrical permitivity, 8·5, effective mass, $0{\cdot}25m_o$, grain size, 9·8 μm, grain resistivity, 1 Ω cm, and Richardson constant, 30 A cm^{-2}K^{-2}

Temperature (°C)	$E_g(eV)$	$\epsilon_\xi(eV)$	$N_D(m^{-3})$	$E_{Fo}(eV)$	$\Phi_{Bo}(eV)$	$Q_{io}(m^{-2})$
19	3·206	0·103	$1{\cdot}432 \times 10^{24}$	2·349	0·754	$3{\cdot}176 \times 10^{16}$
62	3·165	0·124	$1{\cdot}441 \times 10^{24}$	2·243	0·798	$3{\cdot}278 \times 10^{16}$
81	3·147	0·134	$1{\cdot}542 \times 10^{24}$	2·199	0·814	$3{\cdot}426 \times 10^{16}$
100	3·129	0·144	$1{\cdot}804 \times 10^{24}$	2·158	0·827	$3{\cdot}736 \times 10^{16}$
120	3·110	0·154	$2{\cdot}223 \times 10^{24}$	2·114	0·842	$4{\cdot}184 \times 10^{16}$
140	3·091	0·165	$2{\cdot}084 \times 10^{24}$	2·068	0·859	$4{\cdot}090 \times 10^{16}$
160	3·072	0·175	$2{\cdot}395 \times 10^{24}$	2·025	0·872	$4{\cdot}419 \times 10^{16}$

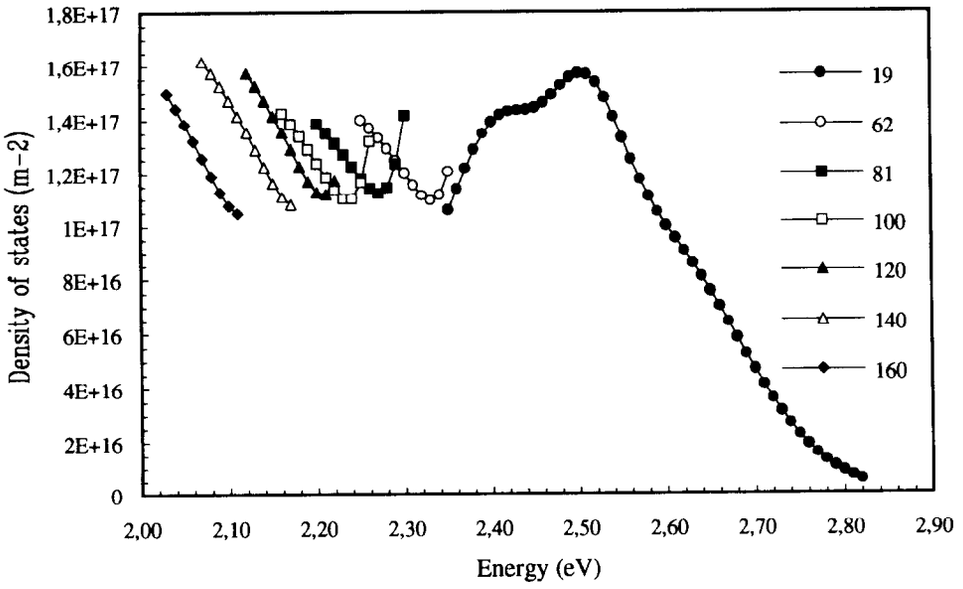

Fig. 6. Energy distribution of surface states (DOS) at various temperatures.

be emphasized that these are guideline parameters and not absolute ones, as pointed out above. The DOS curves in Fig. 6 start at the interface equilibrium energy, E_{Fo}, and end at the energies corresponding to the last experimental point of the I–V curves. Because of this, the room temperature DOS curve is the one with more complete information about the energy distribution. This curve is composed of three main relative peaks, E_2, E_3 and E_4, in Table 2. Their origin is not discussed here, and will be the subject of a forthcoming paper. Although not evident in Fig. 6, with rising temperature, the peaks shift their energy position to lower energies at different rates, and tend to merge together (see Table 2). However, their magnitudes remain unchanged. This observation, together with the linear decrease of E_{Fo}, explains why the values of N_D (Table 1) increase slightly with temperature: as the temperature is rising, some more surface states are being ionized, since they are now below the equilibrium Fermi level, and, to maintain the electrical neutrality condition, eqn (2), N_D must increase. If this behaviour can be extrapolated for higher and lower temperatures, one would expect the following situations:

(i) for higher temperatures, one should see the decrease of the non-ohmic behaviour, since the unionized surface states tend to decrease, and, for some very high temperatures, the system should be ohmic. This behaviour has been experimentally described in the literature;[30,37]

(ii) for lower temperatures, more surface states will be above the equilibrium Fermi level, that is, the sample will show more pronounced varistor characteristics. Concomitantly, there is a higher probability of minor carrier generation by the impact ionization mechanism (or tunneling of electrons from one grain to the other, at the junction). This corresponds to a 'cut-off' of the higher energy surface states, giving the origin of a 'knee' in the I–V curve, or a sharp transition to the breakdown regime. This, in fact, corresponds to much higher α values, that is, the varistor will show α values higher than one could predict *a priori*.[38]

Table 2. Parameters used for the Gaussian curves that describe the DOS for each temperature: E_i, σ_i, and N_i, are the energy level, the standard deviation, and the total surface states, respectively. E_i shift their energy and tend to merge together, while σ_i and N_i remain constant throughout the temperature range. The E_i energies are related to the top of the valence band edge ($E_{VB} = 0$)

Temperature (°C)	*E_1(eV)*	*E_2(eV)*	*E_3(eV)*	*E_4(eV)*
19	2·12	2·41	2·51	2·58
62	2·07	2·28	2·40	2·46
81	2·05	2·21	2·34	2·40
100	2·01	2·14	2·25	2·34
120	1·97	2·05	2·17	2·25
140	1·94	2·00	2·13	2·20
160	1·89	1·92	2·08	2·15
σ_i(eV)	0·15	0·07	0·03	0·10
N_i(m^{-2})	$2{\cdot}9 \times 10^{16}$	$1{\cdot}9 \times 10^{16}$	$4{\cdot}0 \times 10^{15}$	$2{\cdot}3 \times 10^{16}$

It is important to have these observations in mind when attempting to characterize the DOS. In one hand, it is necessary to go to lower temperatures to split the relative peaks of the DOS; on the other hand, at low temperatures some of the DOS will not be 'detected' by the method, namely those at the highest energies. So, the characterization of the DOS is not a straightforward task.

Another important result is the observation that the concentration of donor species in the bulk of

the ZnO grains, is controlling the equilibrium Fermi level at the interface, at least in the temperature range of this work. It is expected that the higher the bulk donor concentration, the lower the temperature coefficient of E_{Fo}, and, since dE_g/dT is constant, this situation leads to a decrease of $E_A = \epsilon_\xi + \Phi_{Bo}$ (E_A is normally determined by the variation of the low voltage ohmic resistivity with temperature, i.e. $\rho = \rho_0 \exp(E_A/kT)$). This means that, unless two different systems are equivalent in their bulk donor concentration, there is no reason to compare the experimentally determined E_A energies in different varistor systems. This is the reason why there is a large range of the determined values for E_A in the literature, $0{\cdot}35 \leq E_A \leq 0{\cdot}94$ eV,[30,39] all of them corresponding to acceptable varistor characteristics.

If the change of E_{Fo} with temperature is only due to the simultaneous variation of E_g and ϵ_ξ, one can extrapolate this result to higher temperatures, and predict what would happen after E_{Fo} reaches the middle of the energy gap, $E_g/2$. For our sample, this situation would happen at ~450°C. Two hypotheses can be considered, either the energy of E_{Fo} continues to decrease after this temperature has been reached, and will be now under the $E_g/2$ value, or E_{Fo} stays at the energy of $E_g/2$.

The first hypothesis would then correspond to a situation where the interface is best described as a p-type semiconductor, while the bulk of the material is still a n-type semiconductor. The junction would then be of the n–p–n type, and, consequently, it would show varistor properties, even at very high temperatures. This is contrary to what has been experimentally observed and reported in the literature.[30,37] The prevision was, of course, a forced one, because even in a p-type semiconductor, at very high temperatures, the Fermi level will tend towards the middle of the band gap, especially if the acceptor concentration is low. However, it must be pointed out that to achieve a p-type conductivity in ZnO, it is necessary to sinter the material at very high oxygen partial pressures,[40,41] or to dope the material with acceptor species. The first condition is not observed in practice, even if one assumes that the Bi-rich liquid phases are good oxygen carriers,[42] since the maximum attainable oxygen partial pressure is *a priori* established by the ambient atmosphere. The second condition can only be observed if the acceptor species are intrinsic in origin, since all the normally used dopants are of the donor type (three- or four-valent cations). The possible intrinsic acceptor species are the interstitial oxygen or the zinc vacancy, the later being invoked, since at the sintering temperatures the Schottky pairs are the predominant defects.[43,44] A surplus of zinc vacancies, or, equivalently, a depression of oxygen vacancies, can arise by the doping process via

$$M_2O_3 \xrightarrow{ZnO} 2M^{\bullet}_{Zn} + 3O_O + V''_{Zn} \qquad (10(a))$$

or

$$M_2O_3 + V_O^{\bullet\bullet} \xrightarrow{ZnO} 2M^{\bullet}_{Zn} + 3O_O \qquad (10(b))$$

(where V_{Zn}'' and $V_O^{\bullet\bullet}$ are the zinc and oxygen vacancy, respectively, both completely ionized, $M_{Zn}^{\bullet}$ is the substitution of a zinc site by the dopant cation, and O_O is an oxygen in its normal site in the ZnO matrix) that is, if the dopants are segregated to the grain boundaries (e.g. M = Bi), it is possible that the interface acts like a p-type semiconductor.

A second hypothesis to consider after E_{Fo} has reached the middle of the band gap, is that it stays at this position when the temperature increases. The interface would then be best described as a n–i–n type junction, where i denotes intrinsic electrical behaviour, or, since the density of majority carriers (electrons) is lower at the interface, it could also be described as a n–insulator–n junction. This model predicts that, at sufficiently high temperatures, the energy difference between the Fermi level and the bottom of the conduction band in both the interface and the bulk of the material, i.e. the barrier height, tends to disappear, and the material will show ohmic behaviour. This is what has been experimentally observed.[30,37] To have intrinsic behaviour at the interface, it is necessary that the material has neither donor nor acceptor levels, or that the net balance of them is null. It is quite unreasonable that there are no defect levels at the interface, since dopants are segregated there from the very beginning of the cooling of the samples.[19] At the sintering temperatures, the Schottky pairs dominate the defect chemistry of the system,[43,44] and, if eqns (10(a, b)) is valid for the formation of associated defects, $(M^{\bullet}_{Zn} - V''_{Zn} - M^{\bullet}_{Zn})^x$, rather than for unassociated species, the condition of net null charge at the interface only requires the annihilation of both oxygen and zinc vacancies following their chemical reaction (Schottky pair equation), during cooling. The elimination of both defects at the interface during cooling, has been the basis for the surface oxidation process.[3,4] Although the formation of the above mentioned associated defects is speculative, it must be emphasized that they could limit the density of unpaired species to a certain extent, which would explain the discrepancy between the density of charged interface defects (10^{12}–10^{13} cm^{-2}) and the concentration of foreign atoms at the interface (~10^{15} cm^{-2}, for Bi atoms), as pointed out by Greuter and Blatter.[20,21]

The second hypothesis discussed above, would

mean that there could be a significant contribution of the surface oxidation process for the barrier height formation. Mahan[42] concluded that the contribution of this process is negligible, ~0·10 eV, which is 10–20% of the total barrier height. Taking his own results (pure ZnO), we have calculated the temperature in which the bulk defects should be frozen, to give $n = 4{\cdot}5 \times 10^{16}$ cm^{-3} at room temperature, and found $T \approx 1050$°C. This seems to be a rather low temperature, since samples quenched from higher temperatures already show varistor characteristics.[19] Taking into consideration that these calculations are reported for pure ZnO, we also calculated the concentration of carriers, n, at the interface, for a frozen temperature of 450°C (temperature at which E_{Fo} in cooling separates from the middle of the band gap), and found $\Delta E_F = kT\ln(n(450°C)/n(1050°C)) \approx 0{\cdot}25$ eV. This contribution can no longer be neglected. Although the contribution of the surface oxidation process, the n–i–n model, to the barrier height formation could then have a significant value, it must be considered that the same type of defect equations (eqns 10 (a, b)) can also be used to explain the contribution to the barrier height formation from a n–p–n model. Subtle differences will be hard to clarify experimentally.

4 Conclusions

Varistor samples sintered at 1300°C in air, developed a microstructure in which the distribution of dopants seemed to indicate that their chemical segregation at the ZnO grain interfaces could be the origin of the electrical potential barrier present in these devices. This type of barrier height formation mechanism should be operative at temperatures below ~950°C, the temperature at which the remaining Bi-rich liquid phase reacts with the spinel phase to give the pyrochlore and ZnO. However, before this temperature most of the ZnO–ZnO grain boundaries are already formed, and the material shows varistor characteristics. Consequently, the contribution of the surface oxidation mechanism to the barrier height formation should only be important at high temperatures, where the diffusion coefficients still allow the migration of the species to the surface of the grains. For temperatures below 950°C, another type of barrier height formation mechanism should then be present.

Taking the double Schottky barrier (DSB) model, we have calculated the distribution of surface states (DOS) above the equilibrium Fermi level for various temperatures, ranging from room temperature up to 160°C. In this temperature range, the equilibrium Fermi level at the interface, E_{Fo}, linearly decreases with temperature, independent of the DOS changes. This variation in relation to the band gap of the semiconductor was assigned to the change of the bulk Fermi level, and so it was possible to derive the density of carriers in the semiconductor conduction band, n. The calculated value, $n \sim 4{\cdot}5 \times 10^{16}$ cm^{-3}, is in good agreement with values, $\sim 1 \times 10^{17}$ cm^{-3}, experimentally determined using other techniques. This procedure can thus be used in any other system, and it also permits the determination of the bulk Fermi level at any temperature. Since the bulk Fermi energy depends on the defect concentration inside the ZnO grains, it is related to the processing of the ceramic, namely to the type and concentration of additives and to the sintering schedule. Consequently, it is expected that each varistor system and processing procedure will give different energy values determined by electrical measurements, which explains the large range of the barrier energy values reported in the literature.

It was also shown that during heating of the samples, the DOS peaks tend to lower energy values, at different rates. This behaviour explains why the interface defect energies also have a large range of reported values. An extrapolation of this behaviour at low temperatures, lead us to the conclusion that the material should show non-linear exponent α at these temperatures, higher than one could predict *a priori*; and also, extrapolating to high temperatures, that the material should show ohmic behaviour.

The temperature dependence of both the band gap of the semiconductor and the energy of the Fermi level, was used to predict the electrical behaviour of the material at high temperatures. The contribution of the surface oxidation mechanism to the formation of the potential barriers, was estimated from the above considerations, and it can be as high as 0·25 eV. According to the results obtained up to now, it seems that the surface states control mainly the shape of the I–V curves. Other contributions to the energy barriers can probably be elucidated by expanding the experimental range of temperatures used to determine the varistor parameters. This is going to be addressed in further publications.

References

1. Pike, G. E. & Seager, C. H., Electronic properties of silicon grain boundaries. In *Grain Boundary Phenomena in Electronic Ceramics*, Advanced Ceramics, Vol. 1, ed. L. M. Levinson. American Ceramics Society, Columbus, Ohio, 1981, pp. 53–66.

2. Pike, G. E. & Seager, C. H., The dc voltage dependence of semiconductor grain boundary resistance. *J. Appl. Phys.*, **50**(5) (1979) 3414–22.
3. Einzinger, R., Grain boundary properties in ZnO varistors. In *Grain Boundary Phenomena in Electronic Ceramics*, Advanced Ceramics, Vol. 1, ed. L. M. Levinson. American Ceramics Society, Columbus, Ohio, 1981, pp. 359–74.
4. Einzinger, R., Grain boundary phenomena in ZnO varistors. In *Grain Boundaries in Semiconductors, Mat. Res. Soc. Symp. Proc.*, Vol. 5, ed. H. J. Leamy, G. E. Pike & C. H. Seager. Elsevier Science Publishers, New York, 1982, pp. 343–55.
5. Bernasconi, J., Klein, H. P., Knecht, B. & Strassler, S., Investigation of various models for metal oxide varistors. *J. Elect. Mater.*, **5**(5) (1976) 473–95.
6. Pike, G. E., Electronic properties of ZnO varistors: A new model. In *Grain Boundaries in Semiconductors, Mat. Res. Soc. Symp. Proc.*, Vol. 5, ed. H. J. Leamy, G. E. Pike & C. H. Seager. Elsevier Science Publishers, New York, 1982, pp. 369–79.
7. Pike, G. E., Kurtz, S. R., Gourley, P. L., Philipp, H. R. & Levinson, L. M., Electroluminescence in ZnO varistors: Evidence for hole contribution to the breakdown mechanism. *J. Appl. Phys.*, **57**(12) (1985) 5512–8.
8. Blatter, G. & Greuter, F., Electrical breakdown at semiconductor grain boundaries. *Phys. Rev. B*, **34**(12) (1986) 8555–72.
9. Blatter, G. & Baeriswyl, D., High-field transport phenomenology: Hot-electron generation at semiconductor interfaces. *Phys. Rev. B*, **36**(12) (1987) 6446–64.
10. Bernasconi, J., Strassler, S., Knecht, B., Klein, H. P. & Menth, A., Zinc oxide based varistors: a possible mechanism. *Solid State Commun.*, **21** (1977) 867–70.
11. Schwing, U. & Hoffman, B., Model experiments describing the microcontact of ZnO varistors. *J. Appl. Phys.*, **57**(12) (1985) 5372–9.
12. Wong, J., Microstructure and phase transformation in a highly non-ohmic metal oxide varistor ceramic. *J. Appl. Phys.*, **46**(4) (1975) 1653–9.
13. Inada, M., Crystal phases of nonohmic zinc oxide ceramics. *Jpn. J. Appl. Phys.*, **17**(1) (1978) 1–10.
14. Inada, M., Microstructure of nonohmic zinc oxide ceramics, *Jpn. J. Appl. Phys.*, **17**(4) (1978) 673–7.
15. Inada, M., Formation mechanism of nonohmic zinc oxide ceramics. *Jpn. J. Appl. Phys.*, **19**(3) (1980) 409–19.
16. Kim, J., Kimura, T. & Yamaguchi, T., Sintering of zinc oxide doped with antimony oxide and bismuth oxide. *J. Am. Ceram. Soc.*, **72**(8) (1989) 1390–5.
17. Olsson, E., Falk, L. K. L., Dunlop, G. L. & Osterlund, R., The microstructure of a ZnO varistor material. *J. Mater. Sci.*, **20** (1985) 4091–8.
18. Kim, J. C. & Goo, E., Morphology and formation mechanism of the pyrochlore phase in ZnO varistor materials. *J. Mater. Sci.*, **24** (1989) 76–82.
19. Mantas, P. Q., Senos, A. M. R. & Bapista, J. L., Varistor–capacitor characteristics of ZnO ceramics. *J. Mater. Sci.*, **21** (1986) 679–86.
20. Blatter, G. & Greuter, F., Carrier transport through grain boundaries in semiconductors. *Phys. Rev. B*, **33**(6) (1986) 3952–66.
21. Greuter, F. & Blatter, G., Electrical properties of grain boundaries in polycrystalline compound semiconductors. *Semicond. Sci. Technol.*, **5** (1990) 111–37.
22. Pike, G. E., Diffusion-limited quasi Fermi level near a semiconductor grain boundary. *Phys. Rev. B*, **30**(6) (1984) 3274–6.
23. Eda, K., Conduction mechanism of non-Ohmic zinc oxide ceramics. *J. Appl. Phys.*, **49**(5) (1978) 2964–72.
24. Tao, M., Ai, B., Dorlanne, O. & Loubiere, A., Different 'single grain junctions' within a ZnO varistor. *J. Appl. Phys.*, **61**(4) (1987) 1562–7.
25. van Kemenade, J. T. C. & Eijnthoven, R. K., Direct determination of barrier voltage in ZnO varistors. *J. Appl. Phys.*, **50**(2) (1979) 938–41.
26. Einzinger, R., Metal oxide varistor action — a homojunction breakdown mechanism. *Appl. Surf. Sci.*, **1** (1978) 329–40.
27. Einzinger, R., Grain junction properties of ZnO varistors. *Appl. Surf. Sci.*, **3** (1979) 390–408.
28. Olsson, E. & Dunlop, G. L., Characterization of individual interfacial barriers in a ZnO varistor material. *J. Appl. Phys.*, **66**(8) (1989) 3666–75.
29. Mukae, K., Tsuda, K. & Nagasawa, I., Capacitance-vs-voltage characteristics of ZnO varistors. *J. Appl. Phys.*, **50**(6) (1979) 4475–6.
30. Matsuoka, M., Nonohmic properties of zinc oxide ceramics. *Jpn. J. Appl. Phys.*, **10**(6) (1971) 736–946.
31. Rossinelli, M., Greuter, F. & Schmückle, F., Electrically active grain boundaries in ceramics: varistors and capacitors. In *Electroceramics, British Ceram. Proc.*, Vol. 41, ed. A. J. Moulson, J. Binner, R. Morell. The Institute of Ceramics, Stoke-on-Trent, U. K., 1989, pp. 177–88.
32. Heilland, G., Mollwo, E. & Stöckmann, F., Electronic processes in zinc oxide. *Solid State Phys.*, **8** (1959) 191–323.
33. Blakemore, J. S., Semiconductor statistics. In *International Series of Monographs on Semiconductors*, Vol. 3, ed. H. K. Henisch. Pergamon Press, Oxford, 1962.
34. Philipp, H. R. & Levinson, L. M., Optical method for determining the grain resistivity in ZnO-based ceramic varistors. *J. Appl. Phys.*, **47**(3) (1976) 1112–26.
35. Levinson, L. M. & Philipp, H. R., High-frequency and high-current studies of metal oxide varistors. *J. Appl. Phys.*, **47**(7) (1976) 3116–21.
36. Hayashi, M., Haba, M., Hirano, S., Okamoto, M. & Watanabe, M., Degradation mechanism of zinc oxide varistors under dc bias. *J. Appl. Phys.*, **53**(8) (1982) 5754–62.
37. Philipp, H. R. & Levinson, L. M., High-temperature behavior of ZnO-based ceramic varistors. *J. Appl. Phys.*, **50**(1) (1979) 383–9.
38. Philipp, H. R. & Levinson, L. M., Low-temperature electrical studies on metal-oxide varistors — A clue to conduction mechanisms. *J. Appl. Phys.*, **48**(4) (1977) 1621–7.
39. Eda, K., Electrical properties of ZnO–Bi_2O_3 metal oxide heterojunction — a clue of a role of intergranular layers in ZnO varistors. In *Grain Boundaries in Semiconductors, Mat. Res. Soc. Symp. Proc.*, Vol 5, ed. H. J. Leamy, G. E. Pike, C. H. Seager. Elsevier Science Publishers, New York, 1982, pp. 381–92.
40. Hagemark, K. I. & Toren, P. E., Determination of excess Zn in ZnO. The phase boundary Zn–$Zn_{1+x}O$. *J. Electrochem. Soc.*, **122** (1975) 992–4.
41. Ziegler, E., Heinrich, A., Oppermann, H. & Stöver, G., Electrical properties and non-stoichiometry in ZnO single crystals. *Phys. Stat. Sol. (a)*, **66** (1981) 635–48.
42. Mahan, G. D., Intrinsic defects in ZnO varistors. *J. Appl. Phys.*, **54**(7) (1983) 3825–32.
43. Göpel, W. & Lampe, U., Influence of defects on the electronic structure of zinc oxide surfaces. *Phys. Rev. B*, **22**(12) (1980) 6447–62.
44. Kröger, F. A., *The Chemistry of Imperfect Crystals*, Vol. 2, 2nd Edn. North-Holland, New York, 1974, p. 743.